Single Source Precursor Approach for the Sol−Gel Synthesis of Nanocrystalline $ZnFe_2O_4$ and Zinc−Iron Oxide Composites

M. Veith,* M. Haas, and V. Huch

Institut für Anorganische Chemie der Universität des Saarlandes, D-66321 Saarbrücken, Germany

Received July 29, 2004. Revised Manuscript Received September 30, 2004

Nanostructured $ZnFe_2O_4$ and zinc oxide−iron oxide composites were obtained by sol−gel processing of a hetero-bimetallic alkoxide. For this purpose the novel molecular precursors $Fe_2Zn(OR)_8$ (R = *t*Bu, ^{i}Pr), fully characterized by spectroscopic and single-crystal diffraction techniques, have been synthesized and their applications in the sol−gel procedure were investigated. The obtained xerogels were annealed at very low temperatures (down to 200 °C) yielding crystalline phases with very small crystallite grain sizes. The phase compositions of the material strongly depend on the polarity of the solvents used in the hydrolysis reaction. When the hydrolysis was performed in the polar propan-2-ol, the spinel $ZnFe_2O_4$ (franklinite) formed at annealing temperature of 200 °C with a mean crystallite grain size D_{vol} of 2.24 nm. However, when using the less polar toluene as solvent in the sol−gel process, iron oxide and zinc oxide are formed together with the franklinite phase. This mixture of phases transforms to the spinel as unique crystalline phase with increasing sintering temperature.

Introduction

Zinc ferrite is well-known within the spinel class to possess a wide range of possible applications and properties such as magnetic behavior, electrical characteristics, and catalytic activity.[1] Spinels have attracted attention for their interesting electrical conductivities,[2,3] and the magnetism of ferrites may be used for magnetic inks, for ferrofluids,[4] and for clinical application.[5] The choice of the synthetic procedure has a direct influence on the formation and the properties of $ZnFe_2O_4$, and especially nanostructured materials exhibiting particular properties[6] due to the extremely low crystallite sizes are still difficult to obtain. New and simple routes toward this material are therefore of great interest.

Attempts to replace standard ceramic methods to monophasic spinel[7] (which need very high calcination temperatures and therefore produce crystals of large sizes) by alternative syntheses are abundant. Frequently, hydrothermal methods with coprecipitation[8] or mechano-synthesis by ball milling[9] are used. These approaches need a mixture of reactants and the spinel is formed only at high sintering temperatures or after long milling. Because of the multiple sources, these materials may contain small amounts of starting material as undesired phases or impurities from the milling process. An alternative approach is the improvement of properties by controlling the arrangement of atoms in the material via positional control.[2,10] In the sol−gel process a *single molecular precursor* may be an alternative to several precursors and several ions, as the molecular building block determines the correct stoichiometry of the final product. The kinetics of the hydrolysis should be simpler as there are less different species in solution and the control of the crystallite grain size could be easier to achieve. The objective of this study is to show our sol−gel process approach using a single source precursor alkoxide for the synthesis of nanocrystalline $ZnFe_2O_4$. Furthermore, the influence of the polarity of the solvent on the sol−gel process has been investigated.

Experimental Section

Preparation of the Single Source Precursors $Zn[Fe(OR)_4]_2$. The alkoxides $[Zn\{Fe(OR)_4\}_2]$ (R = *t*Bu (**1**), ^{i}Pr (**2**)) were prepared

* To whom correspondence should be addressed. E-mail: veith@mx.uni-saarland.de.

(1) El-Nabarawy, Th.; Attia, A. A.; Alaya, M. N. *Mater. Lett.* **1995**, *24*, 319.
(2) (a) Mathur, S.; Haas, M.; Lecerf, N.; Veith, M.; Shen, H.; Hüfner, S.; Haberkorn, R.; Beck, H. P.; Jilavi, M. *J. Am. Ceram. Soc.* **2001**, *84*, 1921. (b) Mathur, S.; Veith, M.; Rügamer, T.; Hemmer, E.; Shen, H. *Chem. Mater.* **2004**, *16*, 1304.
(3) Kim, J.-H.; Yoo, H.-I.; Tuller, H. L. *J. Am. Ceram. Soc.* **1990**, *73*, 258.
(4) (a) Mehtha, R. V.; Upadhyay, R. V.; Dasanacharya, B. A.; Goya, P. S.; Rao, K. S. *J. Magn. Magn. Mater.* **1994**, *132*, 153. (b) Raj, K.; Moskowitz, R.; Casciari, R. *J. Magn. Magn. Mater.* **1995**, *149*, 174.
(5) Østergaard, S.; Blankenstein, G.; Dirac, H.; Leistiko, O. *J. Magn. Magn. Mater.* **1999**, *194*, 156.
(6) Ponpandian, N.; Narayanasamy, A. *J. Appl. Phys.* **2002**, *92*, 2770.
(7) Schiessl, W.; Potzel, W.; Karzel, H.; Steiner, M.; Alvius, G. M.; Martin, M.; Krause, K.; Halevy, I.; Gal, J.; Schäfer, W.; Will, W.; Hillberg, M.; Wäppling, R. *Phys. Rev. B* **1996**, *53*, 9143.
(8) Sato, T.; Haneda, K.; Seki, M.; Iijima, T. *Appl. Phys. A* **1990**, *50*, 13.
(9) (a) Ding, J.; McCormick, P. G.; Street, R. *J. Magn. Magn. Mater.* **1997**, *171*, 309. (b) Bills, I. M. L.; Chatselain, A.; De Heer, W. A. *Science* **1994**, *265*, 1682.
(10) (a) Hench, L. L.; Ulrich, D. R. *Ultrastructure Processing of Ceramics, Glasses and Composites*; Wiley: New York, 1984. (b) Uhlmann, D. R.; Ulrich, D. R. *Ultrastructure Processing of Advanced Materials*; Wiley: New York, 1992. (c) Cheetham, A. K.; Brinker, C. J.; Mecartney, M. L.; Sanchez, C. *Better Ceramics Through Chemistry VI*; Materials Research Society Synopsia Proceedings, 1994 and previous volumes in this series, Vol. 360; Materials Research Society: Pittsburgh, PA, 1994. (d) Interrante, L. V.; Casper, L. A.; Ellis, A. B. *Materials Chemistry − An Emerging Discipline*; Advances in Chemistry Series Vol. 245; American Chemical Society: Washington, DC, 1992. (e) Bruce, D. W., O'Hare, D. *Inorganic Materials*; Wiley: New York, 1992. (f) Stein, A.; Keller, S. W.; Mallouk, T. E. *Science* **1993**, *259*, 1558. (g) Veith, M. *J. Chem. Soc., Dalton Trans.* **2002**, 2405.

10.1021/cm0401802 CCC: $30.25
Published on Web 12/14/2004

under nitrogen, rigorously excluding atmospheric moisture and oxygen. Isopropyl (^{i}Pr) and *tert*-butyl (*t*Bu) alcohols were dried by distillation over sodium metal prior to use. NaO^{i}Pr, NaO*t*Bu, Fe(O^{i}Pr)$_3$, and Fe(O*t*Bu)$_3$ were synthesized according to procedures described in the literature.[11]

*Zn[Fe(OR)$_4$]$_2$ (R = tBu(**1**), ^{i}Pr(**2**)).* To a stirred suspension of either (a) 4.768 g (49.62 mmol) of NaO*t*Bu and 13.626 g (24.74 mmol) of [Fe(O*t*Bu)$_3$]$_2$ in 500 mL of toluene (refluxed for 12h) or (b) a suspension of 15.639 g (49.62 mmol) of NaFe(O^{i}Pr)$_4$ (obtained from the reaction of 16.291 g (198.48 mmol) of NaO^{i}Pr with 8.048 g (49.62 mmol) of FeCl$_3$ in 500 mL of toluene, stirred under reflux for 24 h) 3.382 g (24.82 mmol) of zinc dichloride were slowly added at room temperature. The whole suspension was refluxed for another 12 h, and, after cooling, the solid residue (mostly NaCl) was filtered off. Purification of **1** was achieved by sublimation at 150 °C/10^{-2} mbar, whereas the isopropoxy analogue **2** was distilled at 141 °C/10^{-2} mbar. The overall yields were 16.08 g (85%) for **1** and 11.34 g (60%) for **2**.

Zn[Fe(O*t*Bu)$_4$]$_2$ (**1**). Calcd. for $C_{32}H_{72}Fe_2O_8Zn$ (720.0 g/mol): C, 50.44; H, 9.52; Fe, 14.66; Zn, 8.58. Found: C, 51.10; H, 10.05; Fe, 14.53; Zn, 8.49%. F.p. 197 °C. IR (1300−600 cm^{-1}): 1378st, 1366st, 1356st, 1304w, 1246m, 1223m, 1208m, 1185st, 1021m, 996m, 926st, 781m, 764m. UV−Vis: Broad band (charge transfer) with maximum at 31 250 cm^{-1} (ϵ = 1425 L·mol^{-1}·cm^{-1}). Magnetic moment in toluene: 11.25 μ_B.

Zn[Fe(O^{i}Pr)$_4$]$_2$ (**2**). Calcd. for $C_{24}H_{56}Fe_2O_8Zn$ (649.79 g/mol): C, 44.46; H, 8.69; Fe, 17.19; Zn, 10.06. Found: C, 44.40; H, 8.38; Fe, 17.35; Zn, 9.97%. The liquid turns into a solid on standing.

Instead of using NaO*t*Bu in the reaction with [Fe(O*t*Bu)$_3$]$_2$, also LiO*t*Bu and KO*t*Bu were reacted to form the intermediate Li[Fe(O*t*Bu)$_4$] or K[Fe(O*t*Bu)$_4$]. With 18.81 mmol of [Fe(O*t*Bu)$_3$]$_2$ and an equimolar amount of LiO*t*Bu or KO*t*Bu as starting material either 0.69 g (5%) or 10.17 g (75%) of the final product **1** were obtained.

Alternative route to **2**. A 12.83g (16.8 mmol) portion of Zn[Fe(O*t*Bu)$_4$]$_2$ (**1**) was dissolved in 500 mL of propan-2-ol. The solution was refluxed for 2 h and stirred for 12 h at room temperature. After removal of the alcohol a brown liquid was obtained, which was distilled at 141 °C/10^{-2} mbar to yield 7.66 g (70%) of **2**. Calcd. for $C_{24}H_{56}Fe_2O_8Zn$ (649.79 g/mol): C, 44.46; H, 8.69. Found: C, 44.95; H, 8.98%.

Synthesis of the Ceramics. The isopropoxide derivative **2** is easier to use in the sol−gel process, as it is more readily hydrolyzed compared to the *tert*-butyl compound **1**; nevertheless, both precursors may be used, with the *tert*-butyl derivative presumably changing into the isopropyl one during its contact with propan-2-ol (see above). A solution of Zn[Fe(O^{i}Pr)$_4$]$_2$ (**2**) (Zn[Fe(O*t*Bu)$_4$]$_2$ (**1**)) in either pure propan-2-ol or pure toluene was partially hydrolyzed by slowly adding a saturated solution of water in propan-2-ol over a period of 8 h. The molar ratio of water with respect to the alkoxides **1** and **2** was maintained as 2 to 1. The resulting viscous solution was stirred in air during 10 h and the solvent was evaporated. A brown powder was obtained as residue which was heated in a laboratory furnace at different temperatures to obtain the ceramic material.

Structure Determination and Instrumentation. Needlelike, brown single crystals of **1** were obtained from concentrated solutions of the alkoxide in toluene. A suitable crystal was flame-sealed in a Lindemann capillary and exposed to X-ray diffraction using a STOE-Image-Plate (IPDS, Darmstadt) for recording the intensities of 27 537 (6679 independent) reflections. Using the monoclinic space group $P2_1/n$ with cell dimensions a = 10.163(2) Å, b = 16.856(3) Å, c = 26.189(5) Å, β = 93.44(3)°, V = 4478(1) Å^3, and Z = 4, the crystal structure was solved and refined (268 parameters) to a final R value of R_1 = 0.082.[12] The bad R value is due to disorder of the *tert*-butyl groups. The infrared spectra were recorded using Fourier transform techniques (FTIR model 165, Bio-Rad Laboratories, Krefeld, Germany): the molecular precursors were suspended in Nujol, whereas the gel and the calcinated powders were pressed into KBr pellets. For recording UV−Vis spectra a Lambda 35 spectrometer from Perkin-Elmer was used. The C and H contents of the molecular precursors and of the powders were determined with an elemental analyzer (model CHN 900, Leco Co., St. Joseph, MI) and the metal contents were determined by complexation methods. Powder XRD measurements were performed at room temperature on a diffractometer (model D 5000, Siemens AG, Karlsruhe, Germany) using Co Kα radiation. The average grain sizes and the microstructure were calculated with the help of the FormFit program using essentially a modified Scherrer equation for line broadening.[13] The morphology and the elemental distribution of the powders were studied by scanning electron microscopy (SEM) combined with energy-dispersive X-ray (EDX) analysis (model CAM SCAN S4, Cambridge Instruments, Cambridge, U.K.). Atomic force microscopy was performed on a Nanoscope IV Bioscope (Veeco Instruments, Santa Barbara, CA) in the tapping mode. The microscope was vibration-damped. Ultrashap I-typsilicon cantilevers (NSC16/AIBS, μmasch, Talinn, Estonia), a resonance frequency of about 170 kHz, and a nominal force constant of 40 N/m were used (tip curvature radius <5 nm). The scan speed was proportional to the scan size and the scan frequency was in the range of 0.5−1.5 Hz. The particles were suspended in ethanol (ultrasonic treatment) and the obtained suspension was transferred to a silicon chip by dipping. For the measurement of the magnetic susceptibility in solution of compound **1** an AC-200F Bruker spectrometer (^{1}H (200.13 MHz)) was used with an external diamagnetic reference. The TG-MS measurements of the xerogel were performed on a STA 409 analyzer (Netzsch/Germany). The powders were put into quartz crucibles and heated in air at a rate of 5 K/min in the temperature range 20−1000 °C with an empty quartz crucible as reference.

Results and Discussion

Synthesis and Characterization of Heterometal Precursors 1 and 2. The synthetic procedure to ZnFe$_2$(OR)$_8$ (R = *t*Bu (**1**), ^{i}Pr (**2**)) is summarized in eqs 1−3. In a first step the sodium alkoxide is reacted either with Fe(OR)$_3$ or with iron trichloride to form the alkoxo sodium ferrate which in a subsequent reaction is treated with zinc dichloride to introduce the zinc ion into the molecule. The salt elimination of NaCl seems to be the driving force of the reaction. An alternative procedure to ZnFe$_2$(O^{i}Pr)$_8$ (**2**) is the displacement of *tert*-butyl by isopropyl in compound **1** using an excess of propan-2-ol (eq 3). The *tert*-butoxy derivative **1** is purified by sublimation and the isopropoxy analogue **2** is purified by distillation.

(11) Bradley, D. C.; Mehrotra, R. C.; Gaur, D. P. *Metal Alkoxides*; Academic Press: London, 1978.

(12) (a) Sheldrick, G. M. *SHELXS-86, Program for Crystal Structure Determination*; University of Göttingen: Göttingen, Germany, 1986. (b) Sheldrick, G. M. *SHELXS-97, Program for Crystal Structure Determination*; University of Göttingen: Göttingen, Germany, 1997. Further details of the structure determination may be obtained from the CDCC Cambridge Data file, Cambridge, U.K., on quoting the reference number 257588.

(13) Haberkorn, R. *FormFit-Program for Particle Size Distribution from XRD Scans*; University of Saarland: Saarbrücken, Germany, 2001.

$$NaOR + Fe(OR)_3 \rightarrow NaFe(OR)_4 \quad (1a)$$

$$4\ NaOR + FeCl_3 \rightarrow NaFe(OR)_4 + 3\ NaCl \quad (1b)$$

$$ZnCl_2 + 2\ NaFe(OR)_4 \rightarrow Zn[Fe(OR)_4]_2 + 2\ NaCl$$

R= *t*Bu (**1**), R= ^{i}Pr (**2**) (2)

$$Zn[Fe(O\mathit{t}Bu)_4]_2 + 4\ {}^i PrOH \rightarrow Zn[Fe(O^iPr)_4]_2 + 4\ \mathit{t}BuOH \quad (3)$$

Whereas no single crystals could be obtained from **2**, fine yellow/brown needles of **1** formed which were used for X-ray diffraction.

Instead of NaO*t*Bu, the corresponding lithium and potassium derivatives also have been used in reaction 1 with yields of 5 and 75% for molecule **1** compared to a yield of 90% with the sodium derivative. Apparently the alkali metal has an influence on the reaction product.

The elemental analyses of the molecules **1** and **2** match perfectly with their compositions. The molecules **1** and **2** have been in part characterized by their IR- and UV-spectra, by their magnetic moments, and by an X-ray diffraction study (only for **1**). The FT-IR-spectrum of the precursor **1** shows typical absorptions between 1000 and 1250 cm^{-1} (ν C−O vibration) and bands at 780 and 764 cm^{-1} which may be assigned to M−O stretching. The spectrum in the 800−700 cm^{-1} region is similar to that of $[Fe(O\mathit{t}Bu)_3]_2$ with the exception that most bands are split for **1**. This is mainly due to the two different M−O bond types, as well as to the existence of two different metal ions in the molecule.

In the UV−Vis spectrum no d−d transition bands are found, as Zn(II) has a filled d-shell (d^{10}) and Fe(III) has no allowed d−d transition (d^5, half-filled d-orbitals). Nevertheless, the compound is colored, which comes from a broad absorption band in the near UV with a tail in the visible part of the spectrum (charge transfer occurring between the 3d orbitals of the transition metal and the p_π system of the oxygen-containing ligands[14]).

The magnetic moment of **1** in an organic solution has been determined by NMR using the Evans method[15] as $\mu_{eff} = 11.25\ \mu_B$. This value is very close to the computed theoretical value for 10 unpaired electrons (two noninteracting trivalent iron ions) in the spin-only approach: $\mu_{SO} = [n(n+1)]^{1/2} = 10.49\ \mu_B$. This result indicates that the iron ions separated by $[Zn(O\mathit{t}Bu)^4]^{2-}$ are not, or are only weakly, interacting antiferromagnetically at room temperature and in solution.

In Figure 1 a graphic representation of the molecule $Zn[Fe(O\mathit{t}Bu)_4]_2$ (**1**) is shown as result of a single-crystal diffraction study. Some pertinent bond lengths and angles are collected in the caption of the figure. The molecule has an almost linear Fe···Zn···Fe alignment (Fe−Zn−Fe = 174.2°) and all metal atoms are in the centers of distorted oxygen tetrahedra. Four of the eight *tert*-butoxy ligands are bridging zinc and iron atoms while four others are in terminal positions at the iron atoms. The molecule has approximately D_2 symmetry. The zinc ion has slightly longer bond lengths to oxygen atoms (mean 1.973(8) Å) than the iron atoms to the oxygen atoms of the bridging alkoxo-groups (mean 1.951(8) Å) reflecting presumably the charge difference between the two metal ions. As expected the Fe−O distances to the terminal alkoxo-groups are considerably shorter, which is in accord with the lower coordination numbers at the oxygen atoms (mean 1.783(9) Å), the high thermal elipsoids

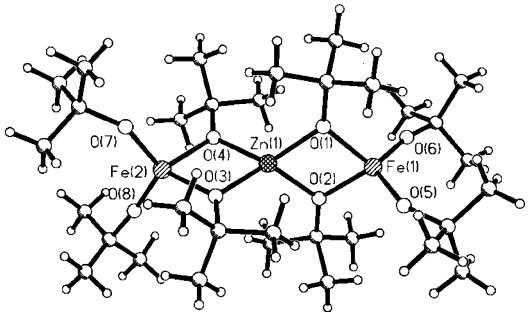

Figure 1. Molecular structure of the precursor $ZnFe_2(O\mathit{t}Bu)_8$. Selected bond length [Å] and bond angles [deg]: Zn(1)−O(1), 1.966(4); Zn(1)−O(2), 1.975(5); Zn(1)−O(3), 1.989(4); Zn(1)−O(4), 1.960(4); Fe(1)−O(1), 1.963(5); Fe(1)−O(2), 1.948(5); Fe(1)−O(5), 1.793(7); Fe(1)−O(6), 1.781; Fe(2)−O(3), 1.936(4); Fe(2)−O(4), 1.956(4); Fe(2)−O(7), 1.798(8); Fe(1)−O(1), 1.761(6); O(1)−Zn(1)−O(4), 125.8(2); O(1)−Zn(1)−O(3), 125.10(18); O(4)−Zn(1)−O(3), 82,15(17); O(1)−Fe(1)−O(6), 113.2(3); O(1)−Fe(1)−O(5), 110.1(3); O(1)−Fe(1)−O(2), 83.51(19); O(6)−Fe(1)−O(5), 119.8(4); Zn(1)−O(1)−Fe(1), 96.53(19); Fe(1)−Zn(1)−Fe(2), 174.28(4).

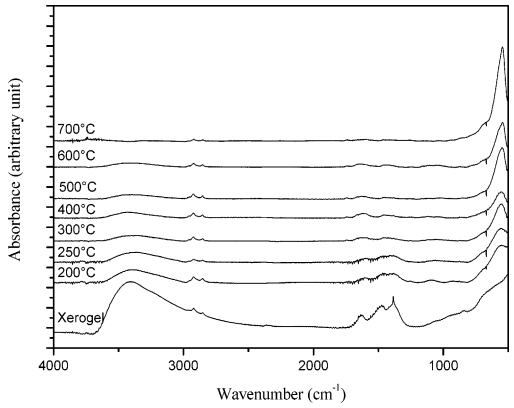

Figure 2. FT-IR spectra of the xerogel and $ZnFe_2O_4$ powders at various annealing temperatures (see text).

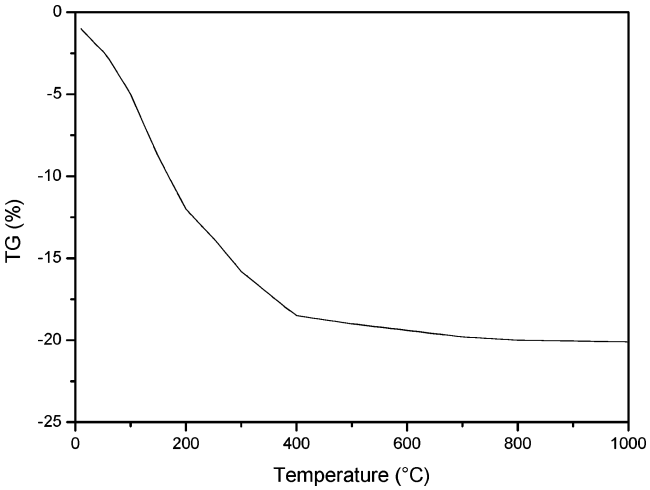

Figure 3. Thermogravimetric profile of $ZnFe_2O_4$ precursor obtained using the sol−gel route of the single source precursor $Zn[Fe(O^iPr)_4]_2$.

(14) Huheey, J. E.; Keiter, E. A.; Keiter, R. L. *Anorganische Chemie*, 2; de Gruyter: Berlin/New York, 1995; p 501.

(15) (a) Evans, D. F. *J. Chem. Soc.* **1959**, 2003. (b) Live, D. H.; Chan, S. I. *Anal. Chem.* **1970**, *42*, 791. (c) Quickenden, T. I.; Marschall, R. C. *J. Chem. Educ.* **1972**, *49*, 114. (d) Hoppee, J. I. *J. Chem. Educ.* **1972**, *49*, 505. (e) Ostfeld, D.; Cohen, I. A. *J. Chem. Educ.* **1972**, *49*, 829. (f) Schubert, E. M. *J. Chem. Educ.* **1992**, *69*, 62.

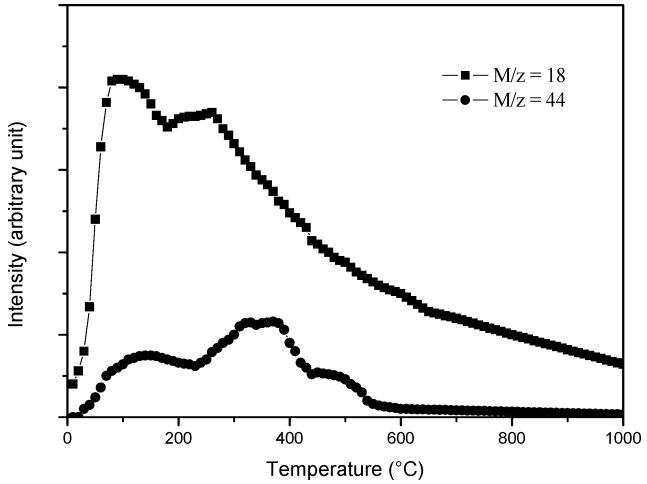

Figure 4. Mass spectra of the gases formed during the thermal treatment of $ZnFe_2O_4$ xerogel (compare Figure 3).

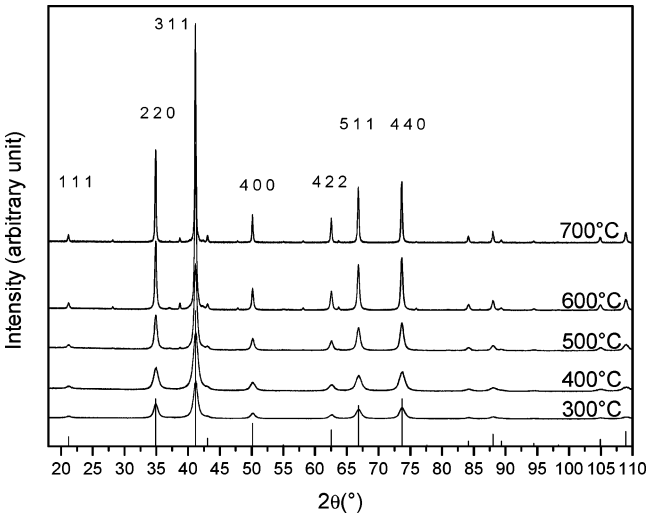

Figure 5. X-ray diffraction pattern of nano-$ZnFe_2O_4$ at various annealing temperatures. On the bottom the bars correspond to bulk $ZnFe_2O_4$ (franklinite).[18] The indexing also corresponds to Franklinite.

of the oxygen and carbon atoms, and consequently large Fe−O−C angles (mean 161(4)°). The inter-planar angle of the two almost planar four-membered ZnO_2Fe rings (dihedral angles 1.9 and 5.1°) is 80°.

Characterization of the Xerogel Intermediate in Propan-2-ol as Solvent and of the Calcinated Powders. The elemental analysis of the xerogel obtained by hydrolysis of a propan-2-ol solution of **2** (or **1**) with water saturated propan-2-ol shows most of the isopropoxy groups in the material being replaced by hydroxyl groups or by oxygen (Zn, 20.77; Fe, 34.44; C, 3.52; H, 3.05%). On heating to 400 °C the carbon and hydrogen content is reduced to less than 1% (C, 0.45; H, 0,36%) and it almost vanishes at 800 °C (C, 0.052; H, 0.016%).

Using the values above, an approximate formal composition of the crude xerogel may be calculated: $ZnFe_{1.94}(O)_{0.06}(OH)_{7.57}(O^iPr)_{0.31}$. The EDX measurements for Zn, Fe, and oxygen were randomly performed on several spots across the samples. By this method statistical tests may be performed which prove the Zn/Fe ratio within the material to be almost accurately 1:2.[16] The xerogels obtained from hydrolysis of **2** in toluene using again water-saturated

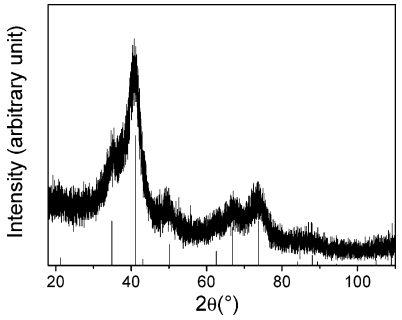

Figure 6. X-ray diffraction pattern of nano-$ZnFe_2O_4$ obtained from the calcination of the xerogel at 200 °C for 24 h. The bars on the bottom correspond to franklinite phase of bulk $ZnFe_2O_4$.[18]

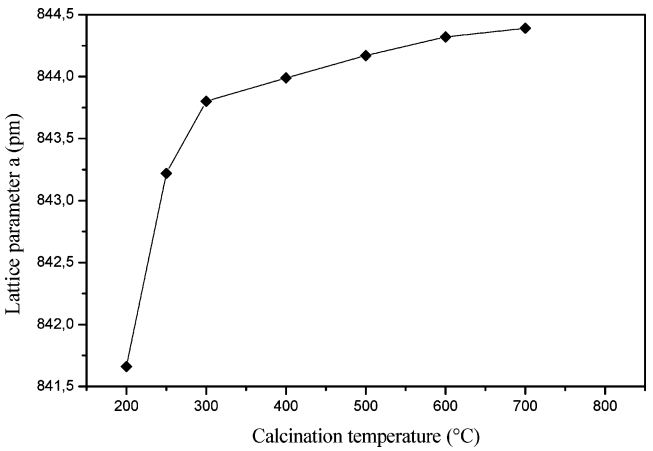

Figure 7. Plot of lattice parameter of $ZnFe_2O_4$ (cubic **a**-axis) versus sintering temperature.

2-propanol (see Experimental Section for exact water content) revealed similar results in the composition.

The FT-IR spectrum (Figure 2) of the xerogel reveals characteristic vibrations of metal-attached hydroxyl (3472 cm^{-1}) and isopropoxyl groups (3000 to 2800 cm^{-1}, 1550 to 1350 cm^{-1}). The absorption band observed at 1635 cm^{-1} is assigned to the deformation vibration of water molecules [$\delta(H_2O)$]. The intensities of υ_{OH} bands (as well as the bands of the alcoholate ligands) decrease on firing the raw material, and at 700 °C no hydroxyl vibration could be detected any more. On the other side, the bands observed in the range from 800 to 500 cm^{-1} (metal oxygen vibrations) increase with rising temperature and become sharper, suggesting an increasing order of the ionic framework. All observations are corroborated by the elemental analysis of the samples and by comparing to values given in the literature.[17]

In Figure 3 a thermo-gravimetric curve (mass loss against temperature) and in Figure 4 the mass isobars of the generated gases for selected mass numbers of the xerogel obtained from hydrolysis in water-saturated propan-2-ol are depicted. From the thermogravimetric analysis of Figure 3 the weight loss seems roughly to proceed in three steps. The first decomposition step takes place up to a temperature of 200 °C and involves a weight loss of around 12%, the second step occurs between 200 and 400 °C and causes a weight loss of a further 7%, and the last (rather flat) step occurs

(16) Laviéville, M. *Statistiques et probabilités*; Dunod: Paris, 1996.
(17) Shirai, H.; Morioka, Y.; Nakagawa, I. *J. Phys. Soc. Jpn.* **1982**, *51*, 592.

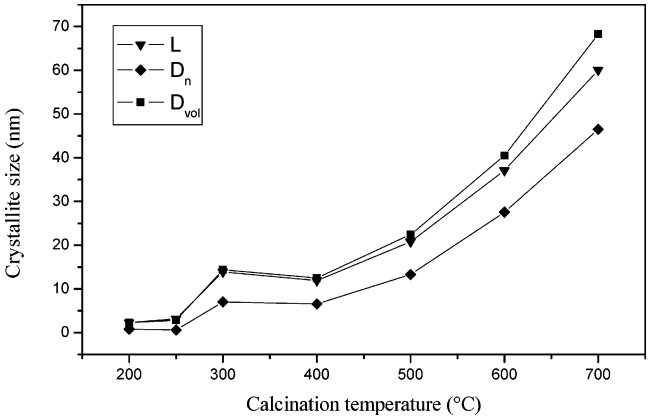

Figure 8. Mean crystallite grain sizes as a function of the calcination temperature with heating duration of 24 h at 200, 250, and 300 °C and 28 h at 400 °C and above: L, mean column height; D_n, mean number weighted grain size; D_{vol} mean volume weighted grain size (error in the attributed sizes between 5 and 15%).

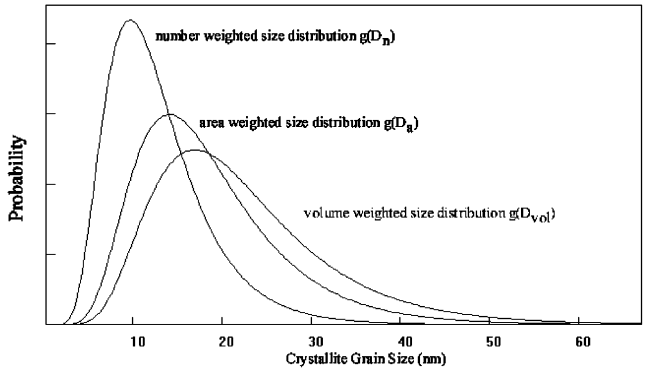

Figure 9. Crystallite grain size distribution of nano-$ZnFe_2O_4$ annealed at 500 °C.

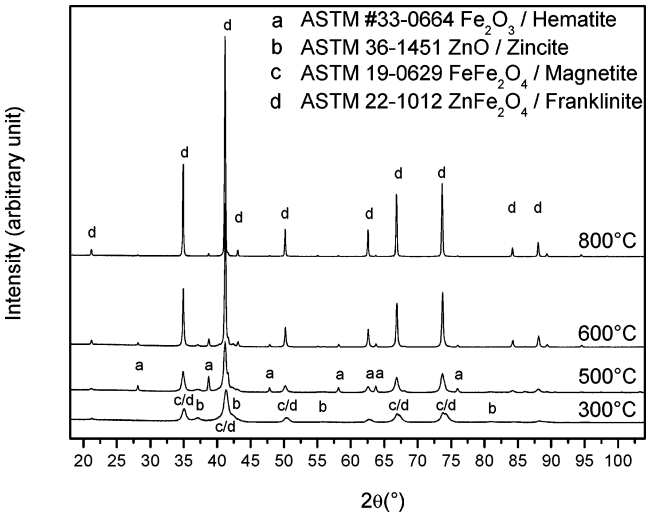

Figure 10. X-ray diffraction pattern of the Zn−O−Fe system (hydrolysis medium: pure toluene + drops of 2-propanol/water) at various annealing temperatures.

above 400 °C with a weight loss of ca. 2%. The overall mass loss of 21% is in the range of the expected weight loss (25%), which can be calculated from the transformation of crude xerogel $ZnFe_{1.94}(O)_{0.06}(OH)_{7.57}(O^iPr)_{0.31}$ (MM 321.7 g/mol, see above) to $ZnFe_2O_4$ (MM 241.1 g/mol). Two different mass/charge ratios were detected in fairly high amounts, as may be deduced from Figure 4, with mass isobars of M/z = 18 and M/z = 44. These values can be assigned to H_2O (for M/z = 18) and CO_2 or propane (for M/z = 44).

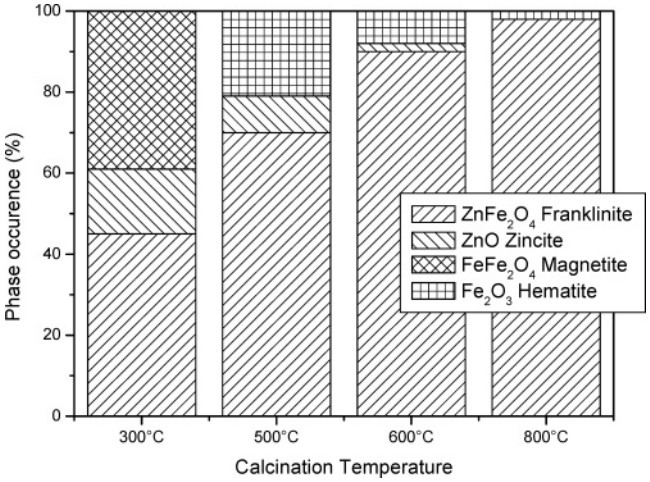

Figure 11. Relative amounts of phases in the Zn−O−Fe system at different annealing temperatures for the hydrolysis (water-saturated 2-propanol) in pure toluene.

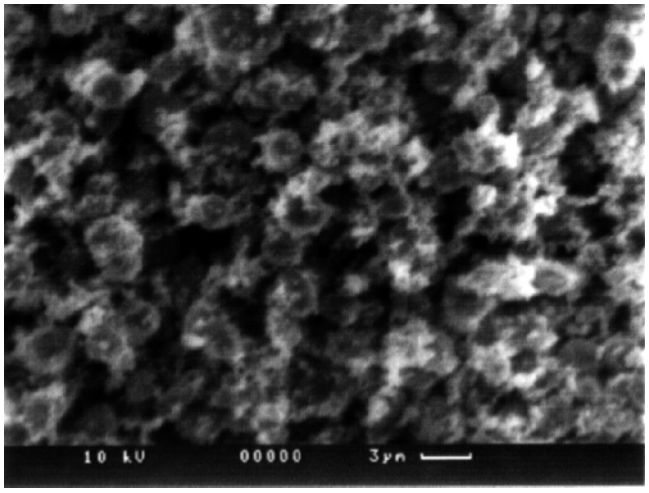

Figure 12. SEM image of $ZnFe_2O_4$ powder annealed at 800 °C.

By comparison of Figures 3 and 4 it is evident that some of the weight losses can be explained by water elimination or by burning steps (CO_2 formation). Especially in the second thermogravimetric step this becomes very evident as the maximum of the H_2O evolution appears at 260 °C and for CO_2 at 350 °C. Also the diminution of water elimination with raising temperature is in accord with the expectation. Interestingly, during these decomposition steps, very low amounts of propan-2-ol could be detected.

The X-ray diffraction patterns obtained from the $ZnFe_2O_4$ xerogel (hydrolysis in propan-2-ol) and from the annealed material are shown in Figure 5. Already at a sintering temperature of as low as 200 °C (Figure 6) some broad reflections of the final $ZnFe_2O_4$ phase[18] can be detected.

This is by far the lowest reported temperature for the crystallization of single-phase $ZnFe_2O_4$ by sol−gel method. Of course at this temperature large amounts of amorphous material are still present, resulting in a high background and low diffraction intensities. With raising calcination temperature the diffraction peaks become sharper, indicating grain growth.

(18) Database PDF 2, Entry 22-1012. International Centre for Diffraction Data: Newtown Square, PA.

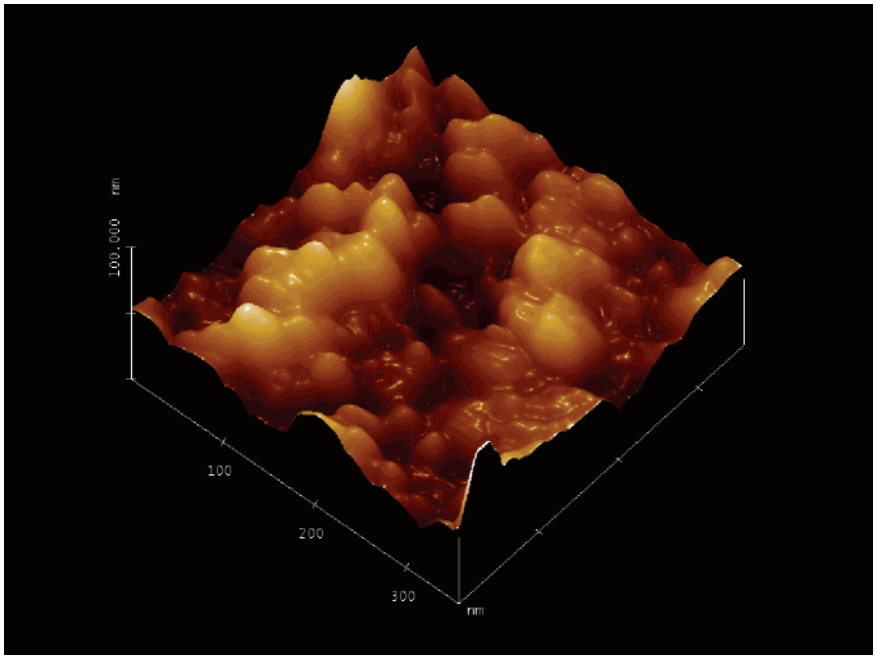

Figure 13. Three-dimensional AFM representation of monophasic $ZnFe_2O_4$ calcinated at 500 °C, scan size 0.35 × 0.35 × 0.10 μm.

The diffraction patterns of the powders were analyzed by FormFit software[19] to get detailed information about the microstructure. The cubic lattice parameter versus firing temperature is plotted in Figure 7. From this plot it becomes clear that the lattice constant increases with increasing sintering temperature to an almost stable value of about 844.3 pm, which is close to that reported for bulk $ZnFe_2O_4$ (844.11 pm).[18] This can be attributed to increasing crystallinity as well as to the ionic ordering within the framework: at low temperatures, the vacancies (e.g., Schottky defects) lead to a smaller lattice constant than that in the bulk material. At the same time, the microstrain ϵ, a parameter which reflects the defects in the ionic assembly, decreases with increasing sintering temperature.

The mean crystallite sizes of the samples as a function of the calcination temperature are shown in Figure 8. The phase obtained at a sintering temperature of 200 °C (Figure 6) is already well crystalline with a number-weighted grain size of just 0.61 nm and a volume-weighted grain size of just 2.84 nm.

The decreasing crystallite grain size of the samples between 300 and 400 °C can be explained by large amounts of amorphous material at lower temperatures which disappear at higher temperatures to produce smaller particle sizes than those at 300 °C.

The grain size distribution of nano-$ZnFe_2O_4$ calcinated at 500 °C is shown in Figure 9 under assumption of a log-normal size distribution empirically verified for most materials.[20,21] This distribution is also corroborated by the grain sizes of this material determined by AFM (see below).

Treatment of $ZnFe_2(OR)_8$ in Nonpolar Solvents. In Figure 10 the diffraction patterns of the powders hydrolyzed (using drops of water-saturated 2-propanol) in the nonpolar toluene are shown for the relevant calcination temperatures of 300, 500, 600, and 800 °C in air. At 300 °C calcination temperature, three phases appear, which can be assigned to $ZnFe_2O_4$ (franklinite), Fe_3O_4 (magnetite),[22] and ZnO (zincite).[23] With raising temperature the magnetite phase disappears in favor of Fe_2O_3 (hematite),[24] whereas both other phases are still persistent. At 800 °C the diffraction peaks become sharper and the spinel phase $ZnFe_2O_4$ becomes predominant.

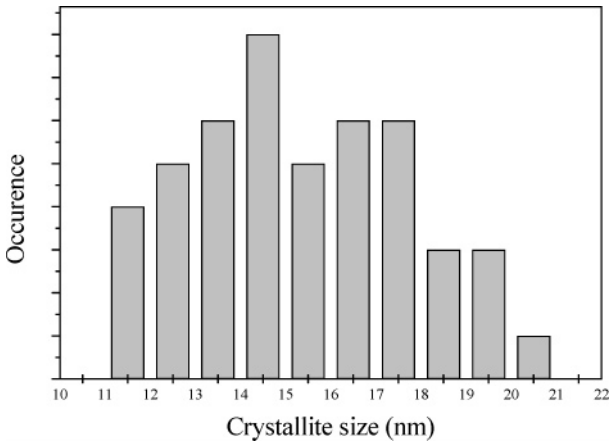

Figure 14. Crystallite size distribution observed by AFM on the sample annealed at 500 °C. On the *y*-axis (occurrence) the numbers of observed grains with the same diameter are given.

The phase compositions in the sol−gel and calcination process using nonpolar toluene/water were derived from the powder diffraction diagrams by a Rietveld analysis with the help of TOPAS software[25] (Figure 11).

(19) Haberkorn, R. *FormFit—A Program for Calculating Microstructure from X-ray Patterns*; Dudweiler: Germany, 2003.
(20) Ngo, A. T.; Bonville, P.; Pileni, M. P. *J. Appl. Phys.* **2001**, *89*, 3370.
(21) Hochepied, J. F.; Pileni, M. P. *J. Appl. Phys.* **2000**, *87*, 2472.
(22) Database PDF 2, Entry 19-0629. International Centre for Diffraction Data: Newtown Square, PA.
(23) Database PDF 2, Entry 36-1451. International Centre for Diffraction Data: Newtown Square: PA.
(24) Database PDF 2, Entry 33-0664. International Centre for Diffraction Data: Newtown Square, PA.
(25) TOPAS V2.0: General profile and structure analysis software for powder diffraction data; Bruker AXS: Karlsruhe, Germany, 2000.

Microscopic Methods. A SEM picture of the monophasic $ZnFe_2O_4$ powder is shown in Figure 12 displaying small particles agglomerated to larger ones. At lower calcination temperatures the particles are even smaller, which can be more easily seen in AFM pictures (for the method see Experimental Section). One of several three-dimensional AFM representations of the sample surface of monophasic $ZnFe_2O_4$ are shown in Figure 13. As in the SEM pictures agglomerates composed of many small crystallites can be recognized clearly.

By a closer look, mean particle sizes of the smallest crystalline grains can be determined leading to a grain size distribution which is displayed in Figure 14 and which follows an almost ideal log-normal distribution (180 repeated measurements of particle diameters at different scan areas using a line scan method merged to 47 unique observables). Using statistical methods a mean diameter of the grains $\langle D \rangle = 14.9 \pm 0.9$ nm can be calculated from these observations, which is fairly close to the value of 13.3 nm evaluated by X-ray diffraction.

Conclusions

The potential of zinc iron alkoxides for applications in material sciences was investigated. Nanocrystalline powders were obtained in a reproducible way. The phase composition of the materials strongly depends on the hydrolysis conditions. It could be shown that the polarity of the hydrolysis medium has an influence upon the phase composition. This effect has been investigated for the $Zn[Fe(O^iPr)_4]_2$ precursor. When the hydrolysis (addition of a small amount of water-saturated propan-2-ol) was performed in the polar propan-2-ol, a monophasic spinel of the type $ZnFe_2O_4$ (franklinite) was obtained at annealing temperatures around 200 °C with a mean crystallite grain size D_{vol} of 2.24 nm. When using pure nonpolar toluene to dissolve the $Zn[Fe(O^iPr)_4]_2$ precursor prior to the same hydrolysis, however, several phases (zinc iron oxide spinel, iron oxide, and zinc oxide) were formed. Iron oxide and zinc oxide phases disappear on heating in favor of the spinel phase.

Thus, the polarity of the hydrolysis medium plays an important role during the sol−gel process. It can be concluded that in nonpolar solvents the single source precursor nature of the alkoxide is not maintained and smaller entities are formed. On the other hand, the polar propan-2-ol seems to stabilize not only the molecular precursor but also the formed intermediates, hence engendering an ideal mixing of the ions on an atomic level when hydrolysis takes place. The result is the generation of monophasic spinels at low calcination temperatures. By careful control of the hydrolysis conditions a minute control of the properties of the products is possible.

Acknowledgment. This work has been supported by the Deutsche Forschungsgemeinschaft in the framework of the international Graduate School 532 and SFB 277 at the University of the Saarland in Saarbrücken. We also thank the Fonds der Chemischen Industrie, and Dr. Haberkorn, University of the Saarland, for assistance in calculations. We thank Prof. U. Bakowsky, Philipps Universität Marburg, Pharmaceutical Technology and Biopharmacie, for the AFM pictures.

Supporting Information Available: Crystallographic information file for the title compound. This material is available free of charge via the Internet at http://pubs.acs.org.

CM0401802